

1 **Future Impact of Differential Inter-Basin Ocean Warming on Atlantic**
2 **Hurricanes**

3
4
5
6
7
8
9
10 Sang-Ki Lee^{1,2}, David B. Enfield^{1,2} and Chunzai Wang²

11 ¹ Cooperative Institute for Marine and Atmospheric Studies, University of Miami, Miami FL

12 ² Atlantic Oceanographic and Meteorological Laboratory, NOAA, Miami FL

13
14
15
16
17 2nd Revision to Journal of Climate

18 October 2010

19
20
21 Corresponding author address: Dr. Sang-Ki Lee, NOAA/AOML, 4301 Rickenbacker Causeway,
22 Miami, FL 33149, USA. E-mail: Sang-Ki.Lee@noaa.gov.

23

1 **Abstract**

2 Global climate model simulations forced by future greenhouse warming project that the
3 tropical North Atlantic (TNA) warms at a slower rate than the tropical Indo-Pacific in the 21st
4 century, consistent with their projections of a weakened Atlantic thermohaline circulation. Here,
5 we use an atmospheric general circulation model to advance a consistent physical rationale that
6 the suppressed warming of the TNA increases the vertical wind shear and static stability aloft in
7 the main development region (MDR) for Atlantic hurricanes, and thus decreases overall Atlantic
8 hurricane activity in the 21st century. A carefully designed suite of model experiments illustrates
9 that the preferential warming of the tropical Indo-Pacific induces a global average warming of
10 the tropical troposphere, via a tropical teleconnection mechanism, and thus increases
11 atmospheric static stability and decreases convection over the suppressed warming region of the
12 TNA. The anomalous diabatic-cooling, in turn, forces the formation of a stationary baroclinic
13 Rossby wave northwest of the forcing region, consistent with the Gill's simple model of tropical
14 atmospheric circulations, in such a way as to induce a secular increase of the MDR vertical wind
15 shear. However, a further analysis indicates that the net effect of future greenhouse warming on
16 the MDR vertical wind shear is less than the observed multidecadal swing of the MDR vertical
17 wind shear in the 20th century. Thus, it is likely that the Atlantic Multidecadal Oscillation will
18 still play a decisive role over the greenhouse warming on the fate of Atlantic hurricane activity
19 throughout the 21st century under the assumption that the 21st century changes in inter-basin
20 SST difference, projected by the global climate model simulations, are accurate.

1 **1. Introduction**

2 Observations during the satellite era of 1965-2005 indicate that a 0.5°C increase of North
3 Atlantic Sea Surface Temperature (SST) in the Atlantic hurricane main development region
4 (MDR; 85°W-15°W, 10°N-20°N) is associated with about a 40% increase in Atlantic hurricane
5 frequency (Saunders and Lea 2008). According to the externally forced model simulations for
6 the 21st century used in the Intergovernmental Panel for Climate Change - 4th Assessment report
7 (IPCC-AR4), the MDR SST may increase by about 2°C or more between 2000 and 2100 due to
8 anthropogenic global warming (AGW). This is alarming given that the MDR SST has never
9 reached such an extremity since reliable and widespread instrumental measurements became
10 available in the late 1800s. At issue is whether we are entering a new era of much elevated
11 hurricane activity due to the rising global SST.

12 In the North Atlantic basin, the most critical environmental factors for hurricane
13 intensification are the MDR vertical wind shear (VWS), which impedes the efficient
14 development of organized convection to increasing heights as the storm intensity increases, and
15 the MDR convective instability of the troposphere (Emanuel, 1994). Thus, both the MDR VWS
16 and convective instability are useful and widely used proxies for overall Atlantic hurricane
17 activity. In this study, the MDR convective precipitation rate (CPR) is used to represent the
18 MDR convective instability.

19 Figure 1 shows the seven-year running-averaged MDR (a) SST anomaly, (b) VWS (200mb
20 minus 850mb) anomaly, and (c) CPR anomaly for the period of 1900-2100 obtained from the
21 ensemble average of 21 IPCC-AR4 climate model simulations under the 20C3M (1900-1999)
22 and A1B (2000-2100) scenarios. The MDR SST increases monotonically by more than 2.5°C
23 between 1900 and 2100. The MDR VWS is characterized by an overall increase with relatively

1 large amplitude of multidecadal variation in the 20th and 21st centuries, whereas the MDR
2 convective instability is significantly reduced between 1900 and 2100. Both the increased MDR
3 VWS and decreased MDR convective instability suggest that Atlantic cyclone activity could be
4 reduced in the 21st century despite an increase in the MDR SST by 2.5°C (Vecchi and Soden
5 2007a). Note that Wang and Lee (2008) also reported a similar upward trend in the observed
6 MDR VWS during a relatively short period of 1949-2006.

7 The upward (downward) trend in MDR VWS (convective instability) and the simultaneous
8 increase in MDR SST are apparently inconsistent with recent research, which shows, based on
9 theory, observations and models, that a warm tropical North Atlantic (TNA) SST is associated
10 with an increase in the MDR convective instability, decreases in the MDR subsidence and sea
11 level pressure, and a weakened tropical upper tropospheric trough circulation, and thus reduces
12 the MDR VWS (Knaff 1997; Knight et al. 2006; Wang et al. 2006; Zhang and Delworth 2006;
13 Vimont and Kossin 2007; Kossin and Vimont 2007). Therefore, it appears that using the
14 observed correlation in the 20th century between the MDR SST and MDR VWS (or convective
15 instability) for projecting Atlantic hurricane activity of the 21st century could be misleading.

16 A newly emerging hypothesis provides us with some insights as to why this may be the case
17 (Latif et al. 2007; Swanson 2008; Vecchi and Soden 2007b; Wang and Lee 2008). The main
18 argument of the hypothesis is that Atlantic hurricanes do not respond to the absolute SST of the
19 MDR but to the SST difference between the MDR and the other tropical ocean basins (hereafter
20 referred to as *differential inter-basin ocean warming hypothesis*). Therefore, it argues that an
21 important and relevant question is if and how the MDR is warming at a different rate from the
22 tropical Indo-Pacific under the AGW scenarios.

1 As shown in Figure 2, the IPCC-AR4 climate model simulations project that the MDR
2 indeed warms at a slower rate than the tropical Indo-Pacific in the 21st century, which is
3 consistent with the projections a weakened Atlantic thermohaline circulation given an apparent
4 coherent relation between the Atlantic thermohaline circulation and the TNA SST (Zhang and
5 Delworth 2005; Timmermann et al. 2007; Zhang 2007; Chiang et al. 2008). It is also noticed that
6 the equatorial Pacific, which is known to be an important region to remotely influence the MDR
7 VWS (Gray 1984; Goldenberg and Shapiro 1997; Latif et al. 2007), warms at a faster rate than
8 the MDR, consistent with the IPCC-AR4 climate model projections of the weakening Pacific
9 Walker circulation (Vecchi and Soden 2007c; DiNezio et al. 2009). Whatever the mechanism
10 that causes the differential inter-basin ocean warming in the IPCC-AR4 climate model
11 simulations, at issue is whether the reduced warming of the MDR is the real cause of the
12 projected secular increase (decrease) of the MDR VWS (convective instability) in the 21st
13 century.

14 To address this important issue, we here explore the atmospheric dynamics that provide
15 physical basis for the differential inter-basin ocean warming hypothesis by performing a set of
16 climate model experiments using an atmospheric general circulation model. Toward the end, we
17 attempt to explain the IPCC-AR4 projected secular increase (decrease) of the MDR VWS
18 (convective instability) in the 21st century by using the causal relationship of the inter-basin SST
19 difference with the MDR VWS (convective instability).

20

21 **2. Model Experiments**

22 The NCAR community atmospheric model version 3 (CAM3) is used as a primary tool for
23 this study. The CAM3 is a global spectral model with a triangular spectral truncation of the

1 spherical harmonics at zonal wave number 85 (T85) and with 26 hybrid sigma-pressure layers.
2 The CAM3 is the atmospheric component of community climate system model version 3
3 (CCSM3), which is one of the climate models used in IPCC-AR4. Model experiments are
4 performed by prescribing various composites of global SST and sea ice fraction, taken from the
5 ensemble average of 11 IPCC-AR4 climate models simulations. The 11 IPCC-AR4 model
6 simulations are selected because they show a consistent upward trend of MDR VWS in the 21st
7 century under the A1B scenario.

8 We have performed three sets of model experiments as summarized in Table 1. In the control
9 experiment (EXP_CTRL), the global SSTs and sea ice fractions are prescribed with twelve
10 monthly climatological values taken from the ensemble average of the 11 IPCC-AR4 climate
11 simulations for the period of 2001-2020. The CO₂ level is fixed to 380ppm, which is the
12 averaged CO₂ level for 2001-2020 under the A1B scenario. Similarly, in the global ocean
13 warming experiment (EXP_GLBW), the global SSTs and sea ice fractions are prescribed with
14 twelve monthly climatological values taken from the ensemble average of the 11 IPCC-AR4
15 climate simulations for the period of 2081-2100. The CO₂ level is fixed to 675ppm, which is the
16 averaged CO₂ level for 2081-2100 under the A1B scenario. Figure 3a shows the SST difference
17 between EXP_GLBW and EXP_CTRL during the Atlantic hurricane season of June to
18 November (JJASON). Comparing EXP_GLBW with EXP_CTRL, the MDR SST is warmer by
19 1.64°C, while the tropical Indo-Pacific (TIP; from east coast of Africa to west coast of the
20 Americas, from the equator to 30°N) SST is warmer by 2.05°C, indicating a 0.41°C per 80yr of
21 differential warming rate between the two regions. Finally, the warmer TNA experiment
22 (EXP_WTNA) is designed to isolate the impact of the suppressed TNA warming. In this
23 experiment, the global sea ice fractions are taken from the ensemble average of the 11 IPCC-

1 AR4 climate simulations for the period of 2081-2100, and the CO₂ level is fixed to 675ppm
2 following the A1B scenario. SSTs in the suppressed warming region of the TNA between the
3 equator and 40°N are increased in such a way that the MDR SST warming is equal to the TIP
4 warming of 2.05°C, whereas the SSTs outside of the suppressed warming region of the TNA are
5 identical to those of EXP_GLBW. See Figure 3 and Table 1 for more details.

6 In each model experiment, the model is integrated for 25 years. The first 10 years of model
7 output are discarded to exclude any possible transient spinup effects. The remaining 15 years of
8 model output are averaged to suppress internal atmospheric variability. To isolate the effects of
9 differential inter-basin ocean warming associated with AGW, the differences between
10 EXP_GLBW and EXP_CTRL, between EXP_WTNA and EXP_GLBW, and between
11 EXP_WTNA and EXP_CTRL are described and compared with the corresponding ensemble
12 average of the 11 IPCC-AR4 climate simulations in the next section.

13 It is important to keep in mind that EXP_WTNA - EXP_GLBW represents a warmer minus
14 cooler TNA. In the case of EXP_GLBW - EXP_CTRL, many forcing factors are represented
15 including (1) global ocean warming, (2) increased greenhouse gas, and (3) suppressed warming
16 of the TNA in contrast to the TIP warming. In the next section, it will be demonstrated that (3) is
17 the only major factor to influence the MDR VWS and convective instability.

18

19 **3. Results**

20 Figure 4a shows the VWS difference between the periods of 2080-2100 and 2000-2020 in
21 JJASON computed from the ensemble average of the 11 IPCC-AR4 climate simulations under
22 the A1B scenario, whereas Figure 4b and 4c show the VWS difference in JJASON between
23 EXP_GLBW and EXP_CTRL, and between EXP_WTNA and EXP_GLBW, respectively. The

1 composite difference in IPCC-AR4 model simulations (Figure 4a) is characterized by an increase
2 in the MDR VWS, particularly over the Caribbean Sea, with averaged amplitude of about 1.6 ms^{-1}
3 in the MDR. The global ocean warming minus control run (Figure 4b) is also characterized by
4 an increased MDR VWS, which is focused over the same region (i.e. the Caribbean Sea) as in
5 the IPCC-AR4 composite difference (Figure 4a) with comparable amplitude. In this case,
6 however, the MDR box-averaged VWS increases only by 0.6 ms^{-1} because the positive VWS
7 change over the Caribbean Sea does not extend into the eastern TNA. In the warmer TNA minus
8 global ocean warming run (Figure 4c), the MDR VWS over the Caribbean Sea is substantially
9 weakened as expected from the earlier studies (Knight et al. 2006; Wang et al. 2006; Zhang and
10 Delworth 2006) with about -1.0 ms^{-1} averaged in the MDR box. This result clearly indicates that
11 the MDR VWS increase in EXP_GLBW - EXP_CTRL could be almost negated if the warming
12 rate of the MDR in the 21st century were as large as that of the TIP. The apparent similarity in
13 the spatial pattern and amplitude of the MDR VWS changes between EXP_GLBW -
14 EXP_CTRL (Figure 4b) and EXP_WTNA - EXP_GLBW (Figure 4c) strongly suggests that the
15 main driver for the MDR VWS increase in EXP_GLBW - EXP_CTRL is the suppressed
16 warming of the TNA in contrast to the TIP. Thus, the differential inter-basin ocean warming
17 response to the AGW explains why a secular increase of MDR SST in the IPCC-AR4 model
18 simulations does not necessarily result in a secular decrease in MDR VWS. We will come back
19 to this point in the later part of this section where we present a consistent physical rationale that
20 supports the differential inter-basin ocean warming hypothesis.

21 To further understand the atmospheric dynamics associated with the MDR VWS changes
22 shown in Figure 4, we now examine the horizontal gradient of geopotential thickness between
23 the upper and lower troposphere, which is dynamically related to VWS via the thermal wind

1 relationship. Figure 5a shows the geopotential thickness and VWS (200mb minus 850mb) vector
2 differences in JJASON between the periods of 2080-2100 and 2000-2020 computed from the
3 ensemble average of the 11 IPCC-AR4 climate simulations under the A1B scenario, whereas
4 Figures 5b and 5c show the geopotential thickness and VWS vector differences in JJASON
5 between EXP_GLBW and EXP_CTRL, and between EXP_WTNA and EXP_GLBW,
6 respectively.

7 The composite difference of the IPCC-AR4 climate model simulations (Figure 5a) is clearly
8 characterized by a region of minimal thickness and cyclonic vertical shear straddling the eastern
9 North Pacific, Central American cordillera and the Gulf of Mexico. The global ocean warming
10 minus control run (Figure 5b) also shows a similar pattern of the geopotential thickness and
11 VWS vector differences, although in this case the Atlantic side of the cyclonic gyre is somewhat
12 separated from the Pacific side by the Sierra Madre and Rocky mountains and much stronger
13 than the Pacific side (The discrepancies between Figure 5a and 5b particularly large over the
14 eastern TNA and North Africa can be attributed to model-to-model variation in response to
15 external SST forcings). The mean atmospheric circulation in boreal summer over the TNA
16 features the easterly trade winds in the lower troposphere and the westerly winds in the upper
17 troposphere. Thus, the wind patterns associated with the baroclinic cyclone strengthen both the
18 lower-tropospheric easterly winds and the upper-tropospheric westerly winds over the Caribbean
19 Sea, resulting in an increase of the MDR VWS.

20 In the case of the warmer TNA minus global ocean warming run (Figure 5c), on the other
21 hand, an intense baroclinic anticyclone is formed in a broad region extending from the eastern
22 North Pacific to the western TNA. The wind patterns associated with the baroclinic anticyclone
23 decrease the MDR VWS. The baroclinic atmospheric response in this case is largely consistent

1 with the Gill's solution to a diabatic-heating in the TNA associated with the prescribed SST
2 pattern (Figure 3b), and thus can be referred to as a heat-induced stationary baroclinic Rossby
3 wave (Gill, 1980). It is immediately noticed that the baroclinic cyclone in EXP_GLBW -
4 EXP_CTRL (Figure 5b) is almost a mirror image to the baroclinic anticyclone in EXP_WTNA -
5 EXP_GLBW (Figure 5c), and thus consistent with the Gill's solution to a diabatic-cooling in the
6 TNA. However, note that the prescribed MDR SST is warmer in EXP_GLBW than in
7 EXP_CTRL by 1.64°C. Apparently, the positive MDR SST forcing in EXP_GLBW -
8 EXP_CTRL is in contradiction with a diabatic-cooling in the TNA.

9 To explain this conundrum, we present the following physical rationale. Even though the
10 TNA SST is warmer in EXP_GLBW than in EXP_CTRL, the overlying atmosphere is also
11 warmed due to the global average tropospheric warming of the tropics, which is largely induced
12 by the increased SSTs in the TIP. In other words, the tropical troposphere tends to respond to
13 surface heating in a zonally symmetric fashion, such that the temperature difference between the
14 troposphere and the differentially heated surface layer (i.e., the atmospheric static instability)
15 will be greater in the TIP and less in the TNA, thus affecting the thickness field as shown in
16 Figure 5. Therefore, in this sense, the suppressed warming of the TNA increases the atmospheric
17 static stability and decreases the convection aloft, and thus evokes a Gill response consistent with
18 local diabatic-cooling.

19 To substantiate this physical explanation, the MDR-averaged atmospheric heating rate
20 (longwave and convective) and pressure velocity from the three CAM3 experiments are plotted
21 in Figure 6. Note that the longwave cooling is increased in both EXP_GLBW and EXP_WTNA
22 from EXP_CTRL, suggesting that the differential inter-basin ocean warming has much smaller
23 impact on radiative cooling of the troposphere aloft of the MDR in comparison to other AGW

1 impacts - a slightly reduced mid-tropospheric longwave cooling in EXP_WTNA from
2 EXP_GLBW can be attributed to the increased MDR convection as suggested in Knaff (1997).
3 On the other hand, the convective heating is much reduced in EXP_GLBW – EXP_CTRL, but
4 not in EXP_WTNA – EXP_CTRL. Consistently, EXP_GLBW – EXP_CTRL is characterized
5 with an enhanced subsidence throughout the entire troposphere aloft the MDR, whereas
6 EXP_WTNA – EXP_CTRL is characterized with a weakly enhanced subsidence only in the
7 upper troposphere possibly associated with the increased radiative cooling in the upper
8 troposphere. The convective precipitation changes shown in Figure 7 also clearly support the
9 physical rationale explained here.

10 A similar argument has been used to explain the observed global tropospheric warming in
11 the tropics associated with the El Niño (e.g. Chiang and Sobel 2002). The physical background
12 for this argument is that atmospheric Kelvin waves tend to redistribute temperature anomalies
13 originating at one particular longitude band over the global tropical strip, which is a very
14 efficient mechanism for tropical teleconnections. Note that the physical rationale provided here
15 is also consistent with Xie et al. (2010) who showed the importance of regional differences in
16 SST warming for tropical convection.

17 In summary, our model experiments clearly demonstrate that the main driver for the
18 increased MDR VWS and decreased MDR convective instability in the IPCC-AR4 climate
19 model simulations for the 21st century is the formation of baroclinic cyclone to the northwest of
20 the MDR, which is a Gill response to a diabatic-cooling associated with the suppressed warming
21 of the TNA in contrast to the TIP.

22

23 **4. Discussions**

1 We now have a consistent physical rationale for expecting a significant relationship between
2 a differential inter-basin ocean warming and the MDR VWS and convective instability in the
3 North Atlantic sector. Naturally, the next question is how well this relationship explains the
4 secular increase (decrease) of the MDR VWS (convective instability) within the 21st century
5 projected by the IPCC-AR4 climate model simulations.

6 Figure 8a shows the time series of reconstructed MDR VWS in JJASON for the period of
7 1900-2100 based on a multiple regression of the MDR VWS onto the MDR SST and TIP SST
8 from the ensemble average of the 21 IPCC-AR4 climate model simulations under the 20C3M
9 and A1B scenarios. The MDR CPR is also reconstructed using the MDR SST and the TIP SST
10 as the predictors for a multiple regression as shown in Figure 8b.

11 A close inspection of Figures 1 and 8 suggests that the original time series and the least
12 squares fits share similar long-term signals and overall trend throughout 1900-2100 period. The
13 least squares equations used for reconstructing MDR VWS and CPR are given by $\text{MDR VWS} =$
14 $-2.7 \times \text{MDR SST} + 3.0 \times \text{TIP SST}$, and $\text{MDR CPR} = 0.9 \times \text{MDR SST} - 1.0 \times \text{TIP SST}$, respectively.
15 These equations confirm that a uniform warming of the MDR SST and TIP SST has little impact
16 on the MDR VWS and convective instability, which are the two most critical environmental
17 factors for Atlantic hurricane activity, and that the inter-basin SST difference is the most
18 important indicator and predictor of Atlantic hurricane activity for both the 20th and 21st
19 centuries, consistent with Vecchi et al. (2008). Multiple linear regressions similar to Figure 8 are
20 also performed for eighteen IPCC-AR4 model simulations, individually. With an exception of
21 only one model simulation, the seven-year running averaged MDR VWS is negatively correlated
22 with the seven-year running averaged MDR SST and positively correlated with the seven-year

1 running averaged TIP SST, confirming the robust relationship between the inter-basin SST
2 difference and the MDR VWS.

3 At the multidecadal or longer time scales, the observed MDR VWS during 1949-2006 period
4 changes by up to 4.0 ms^{-1} (Wang et al. 2008), whereas the ensemble-average of IPCC-AR4
5 model simulations projects that the MDR VWS increases by about 1.0 ms^{-1} in the late 21st
6 century (Figure 1b). Therefore, if the 21st century changes in inter-basin SST difference
7 projected by the IPCC-AR4 model simulations are accurate, the net effect of AGW on the MDR
8 VWS is less than the observed multidecadal swing in the 20th century associated with the
9 Atlantic Multidecadal Oscillation (AMO). Note that the IPCC-AR4 model simulations
10 underestimate the multidecadal swing of the observed MDR VWS in the 20th century because
11 the internally generated multidecadal signals are canceled out after applying the ensemble mean
12 (Knight 2009; Ting et al. 2009).

13 An important and practical question is why the tropical Indo-Pacific warms faster than the
14 TNA in the IPCC-AR4 climate model simulations for the 21st century. Given the existing
15 evidence from research that the cold AMO phase occurs in concert with decreases in the Atlantic
16 thermohaline circulation (e.g. Delworth and Mann 2000; Knights et al. 2006), the suppressed
17 warming of the TNA, in reference to the warming in the tropical Indo-Pacific, is consistent with
18 the IPCC-AR4 projection of a significantly weakened Atlantic Meridional Overturning
19 Circulation (AMOC) in the 21st century – about 25% weaker in the models that produce a
20 reasonable AMOC in the 20th century. Apart from the potential contributions of the weakening
21 AMOC, recent studies by Leloup and Clement (2009), and Xie et al. (2010) provide an
22 alternative explanation for the suppressed warming of the TNA. Their main argument is that a
23 uniform increase of SST may result in a greater evaporative cooling response in the region of

1 high mean surface wind speed such as in the TNA because the mean surface wind speed serves
2 as the efficiency of evaporative cooling response to external forcing. Further studies are
3 warranted to clarify why the IPCC-AR4 climate models project a suppressed warming in the
4 TNA and how reliable that projection is.

5 In this study, we are mainly concerned with secular changes in the Atlantic hurricane
6 climatology in the 21st century using the MDR VWS and CPR from the IPCC-AR4 model
7 simulations as the proxies. However, it is also important to understand the changes in the
8 amplitude of short-term variability especially those associated with El Nino - Southern
9 Oscillation (ENSO, Gray 1984; Goldenberg and Shapiro, 1996), the Atlantic Warm Pool (AWP,
10 Wang et al. 2006; Wang et al. 2008), and Atlantic Meridional Mode (AMM, Vimont and Kossin
11 2007). The IPCC-AR4 model simulations project an increase of about 17% in the amplitude of
12 the MDR VWS at high frequencies (with periods shorter than seven years). Further studies are
13 recommended to explore the changes in ENSO, AWP, and AMM, and their relationships with
14 Atlantic hurricane activity in the 21st century.

15 Finally, there remains another crucial question. Is the suppressed warming of the TNA in the
16 IPCC-AR4 climate model simulations detectable from observed SST records of the 20th
17 century? Unfortunately, we do not have a clear answer to this question because it is difficult if
18 not impossible to cleanly separate the secular trend of observed MDR SST from the multidecadal
19 signal of the AMO, which is the dominant mode of SST variability in the North Atlantic (Enfield
20 and Cid-Serrano, 2010). For instance, during 1901-2008, the Hadley Center sea ice and sea
21 surface temperature (HadISST) and extended reconstructed SST (ERSST3) data give 1.1 and
22 1.5°C per 100 yrs of secular trends of MDR SST, respectively. During the same period, the
23 secular trends of the TIP SST in HadISST and ERSST3 are 1.0 and 1.4°C per 100 yrs,

1 respectively, indicating a preferential warming of the MDR. However, if a positive AMO phase
2 of 1996-2008 is excluded, the secular trends of MDR SST in the HadISST and ERSST3
3 drastically drop to 0.8 and 1.2°C per 100 yrs, respectively, whereas the secular trends of the TIP
4 SST in HadISST and ERSST3 become 0.9 and 1.3°C per 100 yrs, respectively, indicating a
5 suppressed warming of the MDR. An important message here is that the AMO played a decisive
6 role over the AGW on the fate of Atlantic activity in the 20th century, and will continue to do so
7 throughout the 21st century assuming that the net effect of AGW on the inter-basin SST
8 difference, projected by the IPCC-AR4 model simulations, is accurate, and that the AMO is
9 primarily a natural phenomenon, as argued by Enfield and Cid-Serrano (2010).

10

11 **Acknowledgments.** We wish to thank two anonymous reviewers, Eui-Seok Chung, Anthony
12 Broccoli, Brian Mapes, Ben Kirtman, and Frank Marks for thoughtful comments and
13 suggestions. This work was supported by a grant from the National Oceanic and Atmospheric
14 Administration's Climate Program Office and by a grant from the National Science Foundation
15 (ATM-0850897). The findings and conclusions in this report are those of the authors and do not
16 necessarily represent the views of the funding agency.

17

18

References

19 Chiang, J. C. H., and A. H. Sobel, 2002: Tropical tropospheric temperature variations caused by
20 ENSO and their influence on the remote tropical climate. *J. Climate* **15**, 2616-2631.
21 Chiang, J. C. H., W. Cheng, and C. M. Bitz, 2008: Fast teleconnections to the tropical Atlantic
22 sector from Atlantic thermohaline adjustment. *Geophys. Res. Lett.*, **35**, L07704,
23 doi:10.1029/2008GL033292.

1 Delworth, T. L., M. E. Mann, 2000: Observed and simulated multidecadal variability in the
2 Northern Hemisphere. *Climate Dyn.*, **16**, 661-676.

3 Emanuel, K. A., 1994: *Atmospheric Convection*, 580 pp., Oxford Univ. Press, New York.

4 Enfield, D. B., and L. Cid-Serrano, 2010: Secular and multidecadal warmings in the North
5 Atlantic and their relationships with major hurricane activity. *Int. J. Climatol.*, **28**, doi:
6 10.1002/joc.1881.

7 DiNezio, P. N., A. C. Clement, G. A. Vecchi, B. J. Soden, B. P. Kirtman, and S.-K. Lee, 2009:
8 Climate response of the equatorial Pacific to global warming. *J. Climate*, **22**, 4873-4892

9 Gill, A. E., 1980: Some simple solutions for heat-induced tropical circulation. *Quart. J. Roy.*
10 *Meteor. Soc.*, **106**, 447-462.

11 Goldenberg, S. B., and L. J. Shapiro, 1996: Physical mechanisms for the association of El Niño
12 and West African rainfall with Atlantic major hurricane activity. *J. Climate*, **9**, 1169-1187.

13 Gray, W. M., 1984: Atlantic seasonal hurricane frequency. Part I: El Niño and 30 mb Quasi-
14 Biennial Oscillation influences. *Mon. Wea. Rev.*, **112**, 1649–1668.

15 Knaff, J. A., 1997: Implications of summertime sea level pressure anomalies in the tropical
16 Atlantic region. *J. Climate*, **10**, 789–804.

17 Knight, J. R., C. K. Folland, and A. A. Scaife, 2006: Climate impacts of the Atlantic
18 Multidecadal Oscillation. *Geophys. Res. Lett.* **33**, L17706, doi:10.1029/2006GL026242.

19 Knight, J. R., 2009: The Atlantic multidecadal oscillation inferred from the forced climate
20 reponse in coupled general circulation models. *J. Climate*, **22**,1610-1625.

21 Kossin, J. P., and D. J. Vimont, 2007: A more general framework for understanding Atlantic
22 hurricane variability and trends. *Bull. Amer. Meteor. Soc.*, **88**, 1767-1781.

1 Latif, M., N. Keenlyside, and J. Bader, 2007: Tropical sea surface temperature, vertical wind
2 shear, and hurricane development. *Geophys. Res. Lett.* **34**, L01710,
3 doi:10.1029/2006GL027969.

4 Leloup, J., and A. C. Clement, 2009: Why is there a minimum in projected warming in the
5 tropical North Atlantic Ocean? *Geophys. Res. Lett.* **36**, L14802, doi:10.1029/2009GL038609.

6 Saunders, M. A., and A. S. Lea, 2008: Large contribution of sea surface warming to recent
7 increase in Atlantic hurricane activity. *Nature*, **451**, 557-560.

8 Swanson, K. L., 2008: Nonlocality of Atlantic tropical cyclone intensities. *Geochem. Geophys.*
9 *Geosyst.* **9**, Q04V01, doi:10.1029/2007GC001844.

10 Timmermann, A., Y. Okumura, S. I. An, A. C. Clement, B. Dong, E. Guilyardi, A. Hu, J. H.
11 Jungclaus, M. Renold, T. F. Stocker, R. J. Stouffer, R. Sutton, S.-P. Xie, and J. Yin, 2007:
12 The influence of a weakening of the Atlantic meridional overturning circulation on ENSO. *J.*
13 *Climate* **20**, 4899–4919.

14 Ting, M., Y. Kushnir, R. Seager, and C. Li, 2009: Forced and internal twentieth-century SST
15 trends in the North Atlantic. *J. Climate*, **22**, 1469–1481.

16 Vecchi, G. A., and B. J. Soden, 2007a: Increased tropical Atlantic wind shear in model
17 projections of global warming. *Geophys. Res. Lett.* **34**, L08701, doi:10.1029/2006GL028905.

18 Vecchi, G. A., B. J. Soden, 2007b: Effect of remote sea surface temperature change on tropical
19 cyclone potential intensity. *Nature*, **450**, 1066-1070, doi:10.1038/nature06423.

20 Vecchi, G. A., B. J. Soden, 2007c: Global warming and the weakening of the tropical circulation.
21 *J. Climate*, **20**, 4316–4340.

22 Vecchi, G. A., K. L. Swanson, and B. J. Soden, 2008: Whither hurricane activity? *Science*, **322**,
23 doi: 10.1126/science.1164396.

1 Vimont, D. J., and J. P. Kossin, 2007: The Atlantic meridional mode and hurricane activity.
2 *Geophys. Res. Lett.*, **34**, L07709, doi:10.1029/2007GL029683.

3 Wang, C., D. B. Enfield, S.-K. Lee, C. W. Landsea, 2006: Influences of Atlantic warm pool on
4 Western Hemisphere summer rainfall and Atlantic hurricanes. *J. Climate*, **19**, 3011-3028.

5 Wang, C., and S.-K. Lee, 2008: Global warming and United States landfalling hurricanes.
6 *Geophys. Res. Lett.* **35**, L02708, doi:10.1029/2007GL032396.

7 Wang, C., S.-K. Lee, and D. B. Enfield, 2008: Atlantic warm pool acting as a link between
8 Atlantic multidecadal oscillation and Atlantic tropical cyclone activity. *Geochem. Geophys.*
9 *Geosyst.* **9**, Q05V03, doi:10.1029/2007GC001809.

10 Xie, S.-P., C. Deser, G. A. Vecchi, J. Ma, H. Teng, and A. T. Wittenberg, 2010: Global warming
11 pattern formation: Sea surface temperature and rainfall. *J. Climate*, **23**, 966-986.

12 Zhang, R., and T. L. Delworth, 2005: Simulated tropical response to a substantial weakening of
13 the Atlantic thermohaline circulation. *J Climate*, **18**, 1853-1860.

14 Zhang, R., and T. L. Delworth, 2006: Impact of Atlantic multidecadal oscillations on India/Sahel
15 rainfall and Atlantic hurricanes. *Geophys. Res. Lett.* **33**, L17712,
16 doi:10.1029/2006GL026267.

17 Zhang, R., 2007: Anticorrelated multidecadal variations between surface and subsurface tropical
18 North Atlantic. *Geophys. Res. Lett.* **34**, L12713, doi:10.1029/2007GL030225.

19
20
21
22
23

1 **Table 1.** Global SST and sea-ice fraction prescribed in the four CAM3 experiments are obtained
 2 from the ensemble average of 11 IPCC-AR4 climate simulations for the 21st century under the
 3 A1B scenario for the periods described in this table. Also shown in this table are the TIP and
 4 MDR SST increases in each experiment in reference to the control experiment. CO₂ level
 5 specified for the three experiments are also summarized in this table. See text for more detail.

Experiments	TIP SST Increase	MDR SST Increase	Global SST	Sea Ice Fraction	CO ₂ Level
EXP_CTRL	-	-	2001 ~ 2020	2001 ~ 2020	380ppm
EXP_GLBW	2.05	1.64	2081 ~ 2100	2081 ~ 2100	675ppm
EXP_WTNA	2.05	2.05	2081 ~ 2100	2081 ~ 2100	675ppm

6
 7 **Figure 1.** Seven-year running mean (a) SST anomaly, (b) VWS (200mb minus 850mb) anomaly
 8 and (c) CPR anomaly averaged in the MDR (85°W-15°W, 10°N-20°N) for the period of 1900-
 9 2100 obtained from the ensemble average of 21 IPCC-AR4 climate model simulations under the
 10 20C3M (1900-1999) and A1B (2000-2100) scenarios. The period of 1900-1999 is used as the
 11 baseline for computing the anomalies. Gray lines represent 95% significance, which is computed
 12 based on a bootstrap technique.

13
 14 **Figure 2.** Linear trend of SST (in unit of °C per 100 years) in JJASON during 2000-2100 periods
 15 computed from the ensemble average of 21 IPCC-AR4 climate simulations under the A1B
 16 scenario.

17

1 **Figure 3.** SST difference (in unit of °C) in JJASON for (a) EXP_GLBW - EXP_CTRL, and (b)
2 EXP_WTNA - EXP_GLBW. The box region indicates the MDR for Atlantic hurricanes (85°W-
3 15°W, 10°N-20°N). The MDR averaged SST difference between EXP_GLBW and EXP_CTRL
4 is indicated in the upper right corner of (a) along with the SST difference averaged in the TIP
5 (from west coast of Africa to east coast of the Americas, from the equator to 30°N). Similarly,
6 the MDR averaged SST difference between EXP_WTNA and EXP_CTRL is indicated in the
7 upper right corner of (b) along with the SST difference averaged in the TIP.

8
9 **Figure 4.** (a) VWS (200mb minus 850mb) difference in JJASON between 2080-2100 and 2000-
10 2020 periods computed from the ensemble average of 11 IPCC-AR4 climate simulations under
11 the A1B scenario. The VWS difference in JJASON for (b) EXP_GLBW - EXP_CTRL and (c)
12 EXP_WTNA - EXP_GLBW. White areas are mountain regions without 850mb data. The box
13 region indicates the MDR for Atlantic hurricanes.

14
15 **Figure 5.** (a) Geopotential thickness and VWS vector (200mb minus 850mb) differences in
16 JJASON between 2080-2100 and 2000-2020 periods computed from the ensemble average of 11
17 IPCC-AR4 climate simulations under the A1B scenario. Geopotential thickness and VWS vector
18 differences in JJASON for (b) EXP_GLBW - EXP_CTRL and (c) EXP_WTNA - EXP_GLBW.
19 White areas are mountain regions without 850mb data. Dynamic responses of the atmosphere to
20 AGW are most prominent over high-latitudes around 50 ~ 60°N with a significant amplitude in
21 zonally averaged components (not shown). Since the main interest is tropical atmospheric
22 dynamics around the MDR, the zonal mean components of geopotential thickness difference are
23 removed. Note that the zonal means are not removed in VWS difference.

1
2 **Figure 6.** MDR-averaged (a) longwave (Q_L) and (b) convective (Q_C) heating rates and (c)
3 pressure velocity (ω) in JJASON computed from EXP_CTRL, EXP_GLBW, and EXP_WTNA.
4 Changes of (d) Q_L , (e) Q_C , and (f) ω in EXP_GLBW and EXP_WTNA in reference to
5 EXP_CTRL. The pressure velocity is positive upward.

6
7 **Figure 7.** (a) CPR difference (in unit of mm day^{-1}) in JJASON between 2080-2100 and 2000-
8 2020 periods computed from the ensemble average of the 11 IPCC-AR4 climate simulations
9 under the A1B scenario. The CPR difference in JJASON for (b) EXP_GLBW - EXP_CTRL and
10 (c) EXP_WTNA - EXP_GLBW.

11
12 **Figure 8.** Times series of reconstructed (a) MDR VWS and (b) CPR in JJASON for the period of
13 1900-2100 based on multiple regressions of the MDR VWS and CPR onto the MDR SST and
14 TIP SST from the ensemble average of 21 IPCC-AR4 climate model simulations under the
15 20C3M and the A1B scenarios. Seven-year running mean is applied to all indices before
16 applying the multiple regressions.

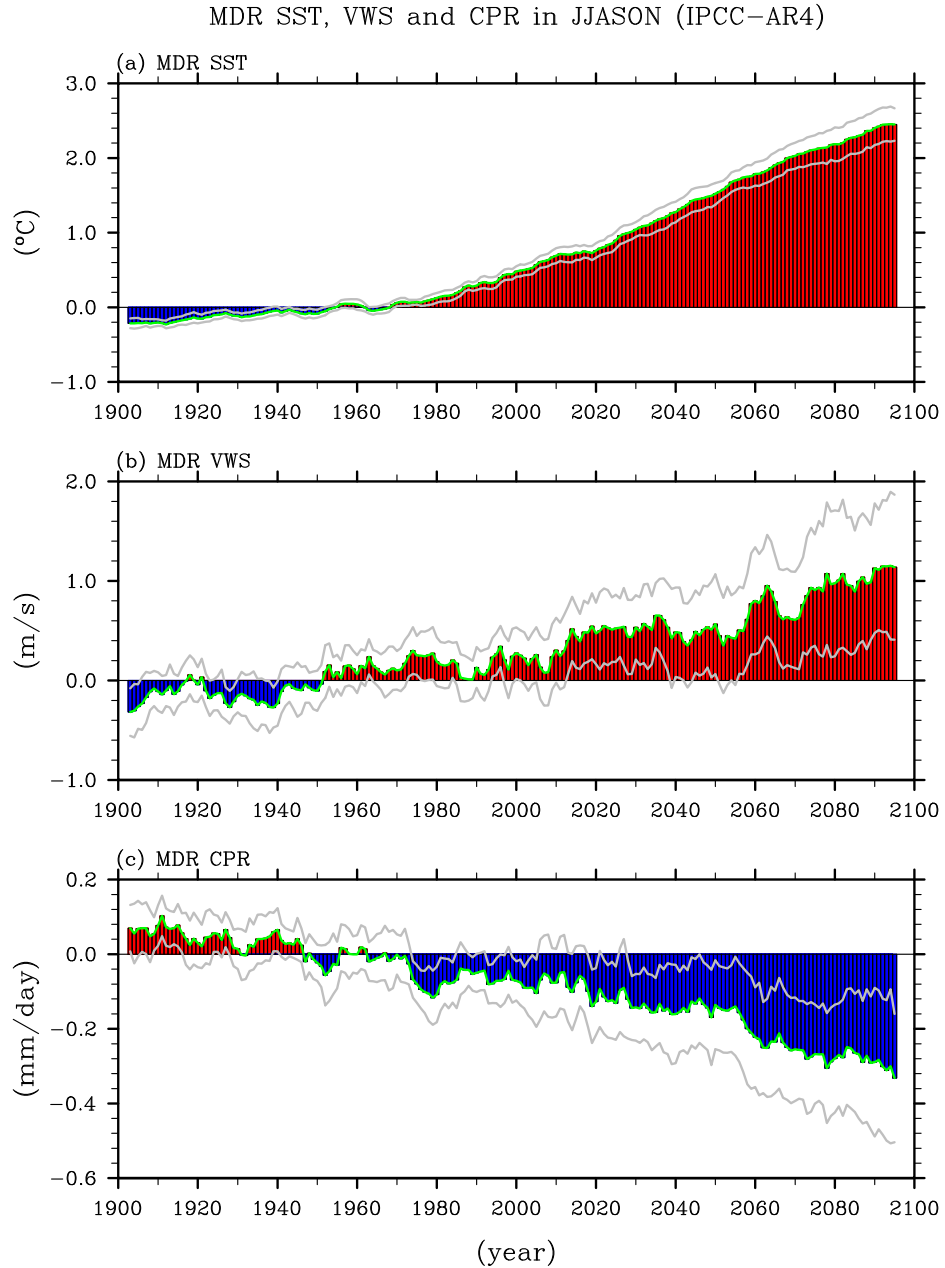


Figure 1. Seven-year running mean (a) SST anomaly, (b) VWS (200mb minus 850mb) anomaly and (c) CPR anomaly averaged in the MDR (85°W - 15°W , 10°N - 20°N) for the period of 1900-2100 obtained from the ensemble average of 21 IPCC-AR4 climate model simulations under the 20C3M (1900-1999) and SRESA1B (2000-2100) scenarios. The period of 1900-1999 is used as the baseline for computing the anomalies. Gray lines represent 95% significance, which is computed based on a bootstrap technique.

Linear Trend of SST in JJASON (IPCC-AR4)

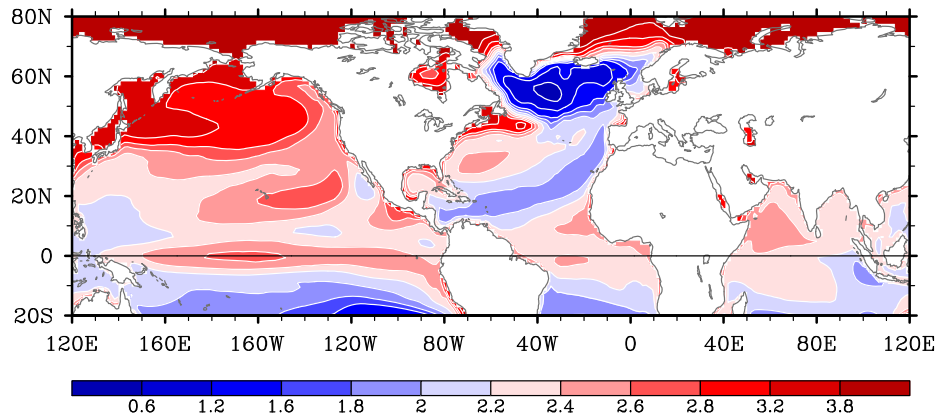


Figure 2. Linear trend of SST (in unit of °C per 100 years) in JJASON during 2000-2100 periods computed from the ensemble average of 21 IPCC-AR4 climate simulations under SRESA1B scenario.

SST Change in JJASON

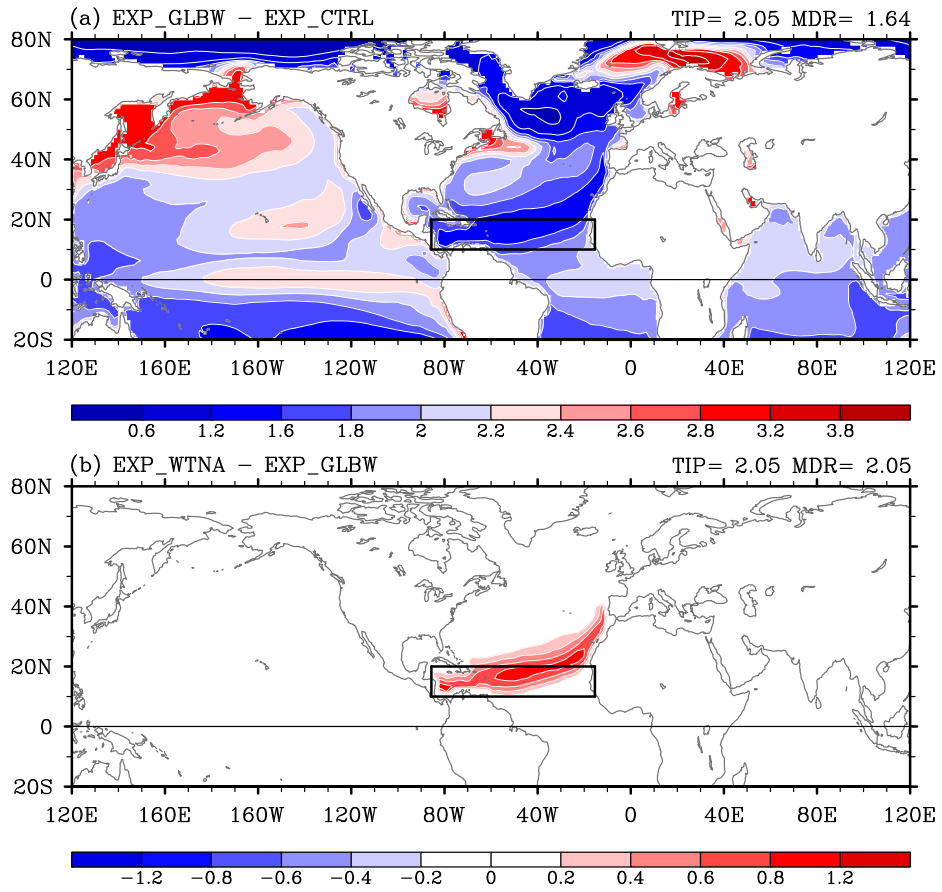


Figure 3. SST difference (in unit of $^{\circ}\text{C}$) in JJASON for (a) EXP_GLBW - EXP_CTRL, and (b) EXP_WTNA - EXP_GLBW. The box region indicates the MDR for Atlantic hurricanes (85°W - 15°W , 10°N - 20°N). The MDR averaged SST difference between EXP_GLBW and EXP_CTRL is indicated in the upper right corner of (a) along with the SST difference averaged in the TIP (from west coast of Africa to east coast of the Americas, from the equator to 30°N). Similarly, the MDR averaged SST difference between EXP_WTNA and EXP_CTRL is indicated in the upper right corner of (b) along with the SST difference averaged in the TIP.

Vertical Wind Shear Change in JJASON

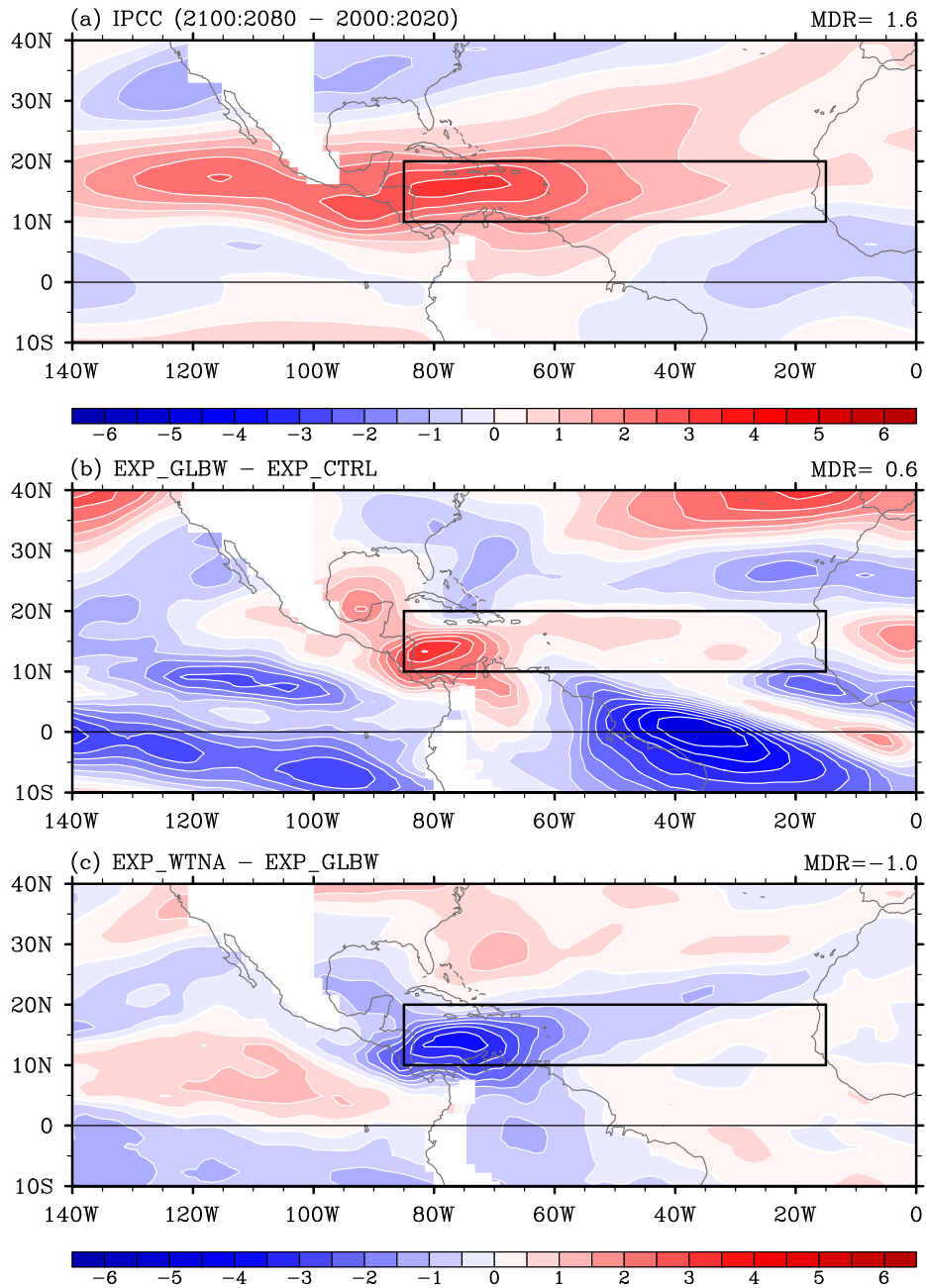


Figure 4. (a) VWS (200mb minus 850mb) difference in JJASON between 2080-2100 and 2000-2020 periods computed from the ensemble average of 11 IPCC-AR4 climate simulations under the SRESA1B scenario. The VWS difference in JJASON for (b) EXP_GLBW - EXP_CTRL and (c) EXP_WTNA - EXP_GLBW. White areas are mountain regions without 850mb data. The box region indicates the MDR for Atlantic hurricanes.

Geopotential Thickness (200 – 850mb) change in JJASON

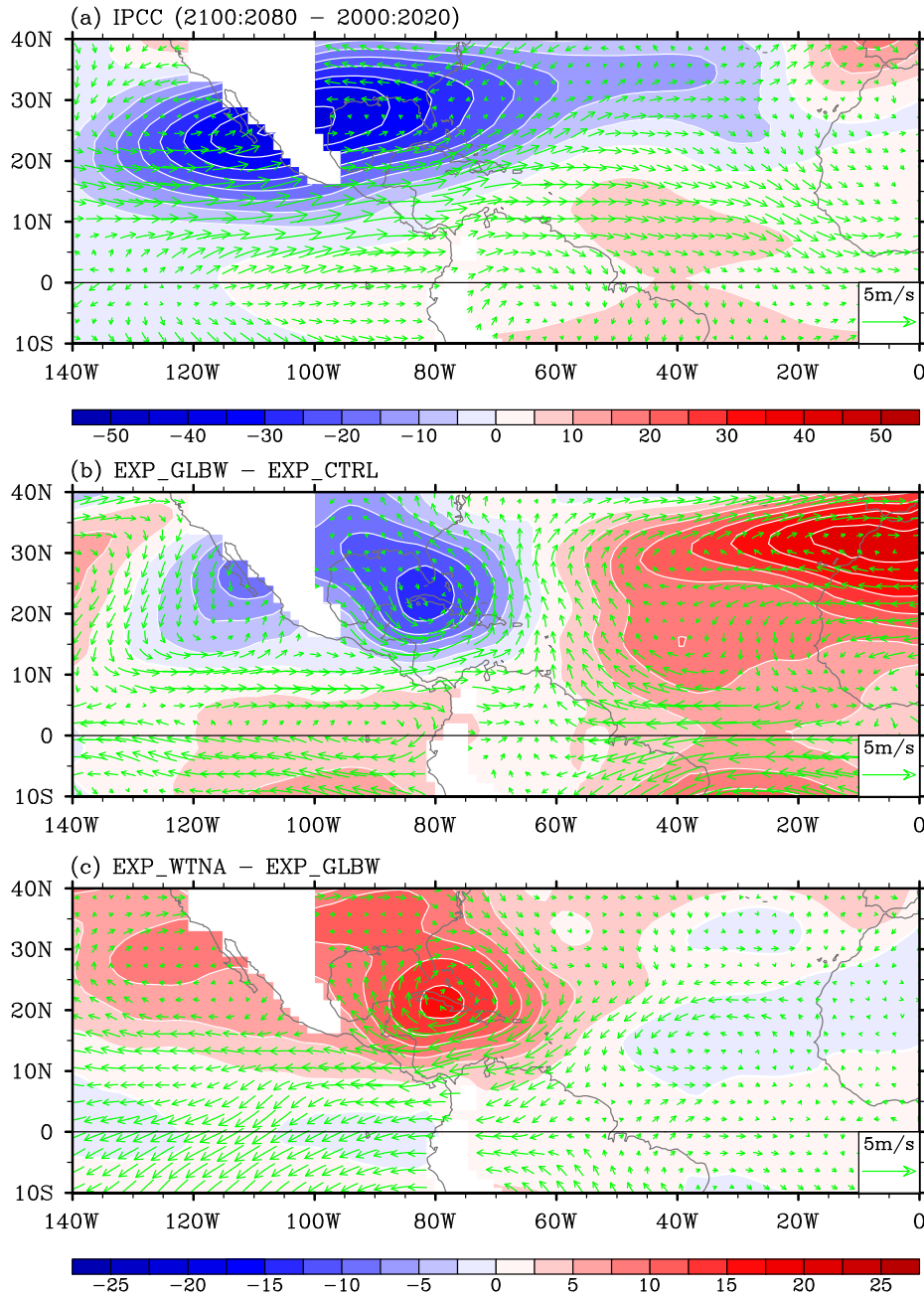


Figure 5. (a) Geopotential thickness and VWS vector (200mb minus 850mb) differences in JJASON between 2080-2100 and 2000-2020 periods computed from the ensemble average of 11 IPCC-AR4 climate simulations under SRESA1B scenario. Geopotential thickness and VWS vector differences in JJASON for (b) EXP_GLBW - EXP_CTRL and (c) EXP_WTNA - EXP_GLBW. White areas are mountain regions without 850mb data. Dynamic responses of the atmosphere to AGW are most prominent over high-latitudes around $50 \sim 60^\circ\text{N}$ with a significant amplitude in zonally averaged components (not shown). Since the main interest is tropical atmospheric dynamics around the MDR, the zonal mean components of geopotential thickness difference are removed. Note that the zonal means are not removed in VWS difference.

MDR-Averaged Heating Rate and Pressure Velocity in JJASON

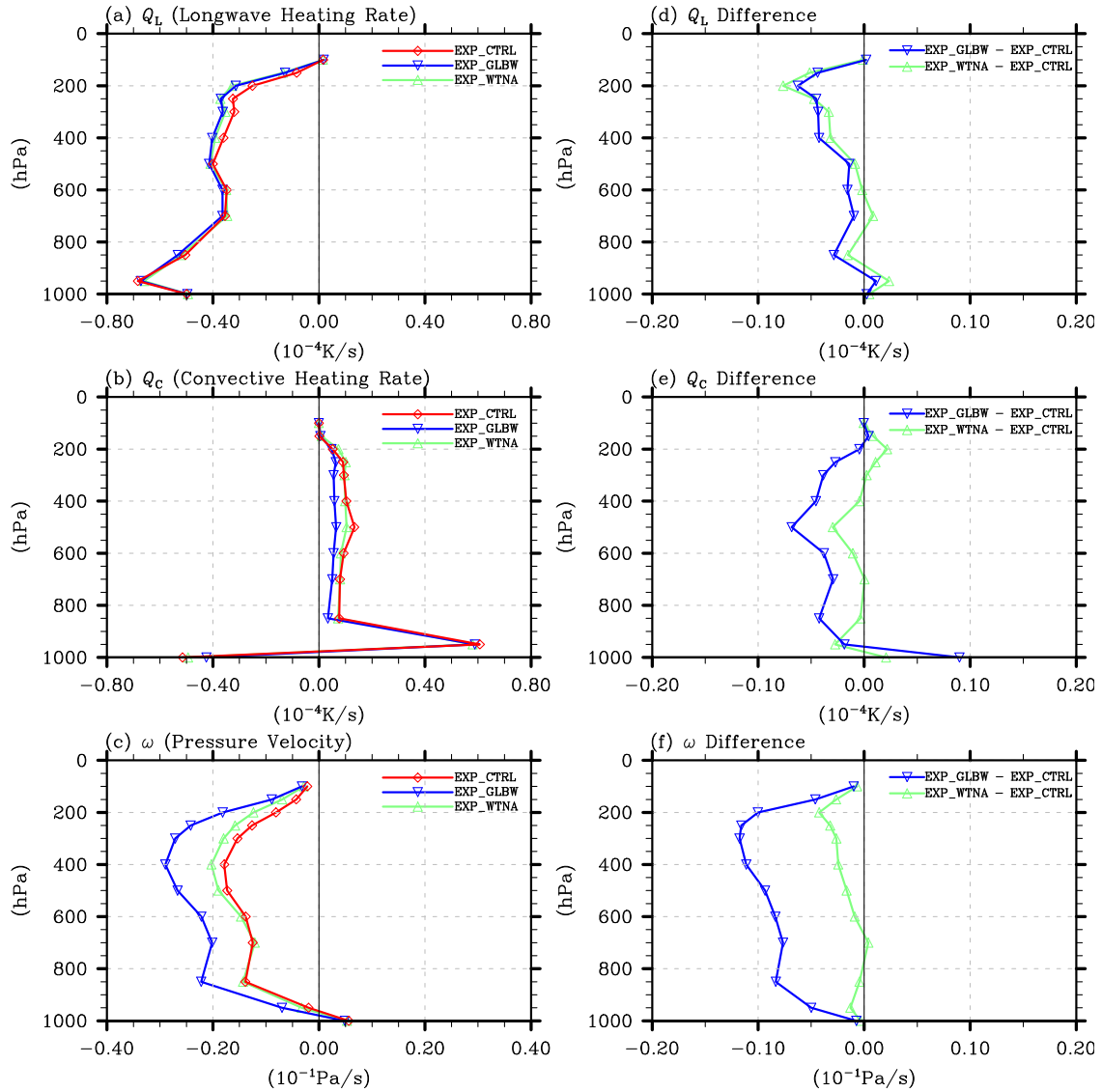


Figure 6. MDR-averaged (a) longwave (Q_L) and (b) convective (Q_C) heating rates and (c) pressure velocity (ω) in JJASON computed from EXP_CTRL, EXP_GLBW, and EXP_WTNA. Changes of (d) Q_L , (e) Q_C , and (f) ω in EXP_GLBW and EXP_WTNA in reference to EXP_CTRL. The pressure velocity is positive upward.

Conv. Prec. Rate Change in JJASON

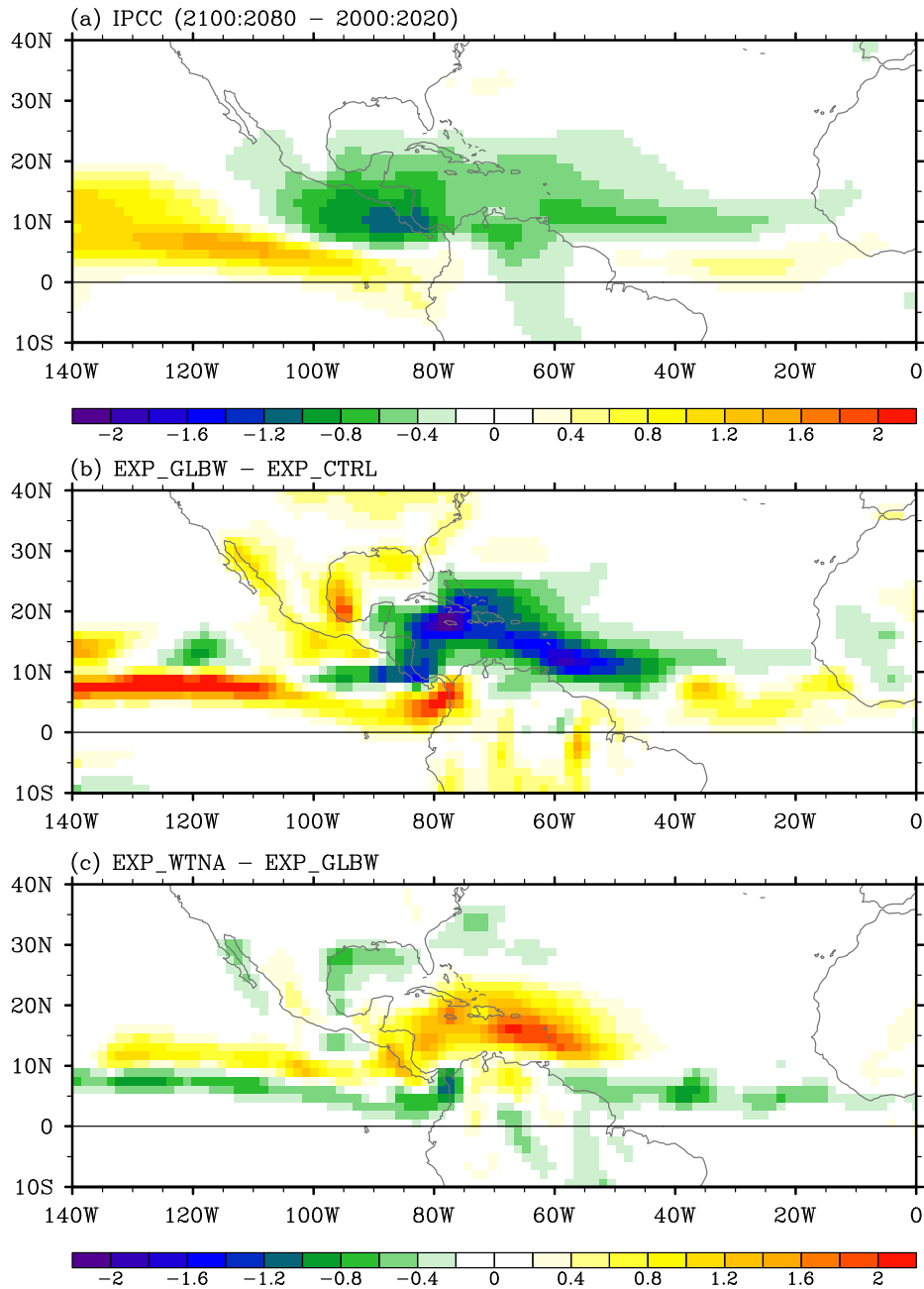


Figure 7. (a) CPR difference (in unit of mm day^{-1}) in JJASON between 2080-2100 and 2000-2020 periods computed from the ensemble average of the 11 IPCC-AR4 climate simulations under SRESA1B scenario. The CPR difference in JJASON for (b) EXP_GLBW - EXP_CTRL and (c) EXP_WTNA - EXP_GLBW.

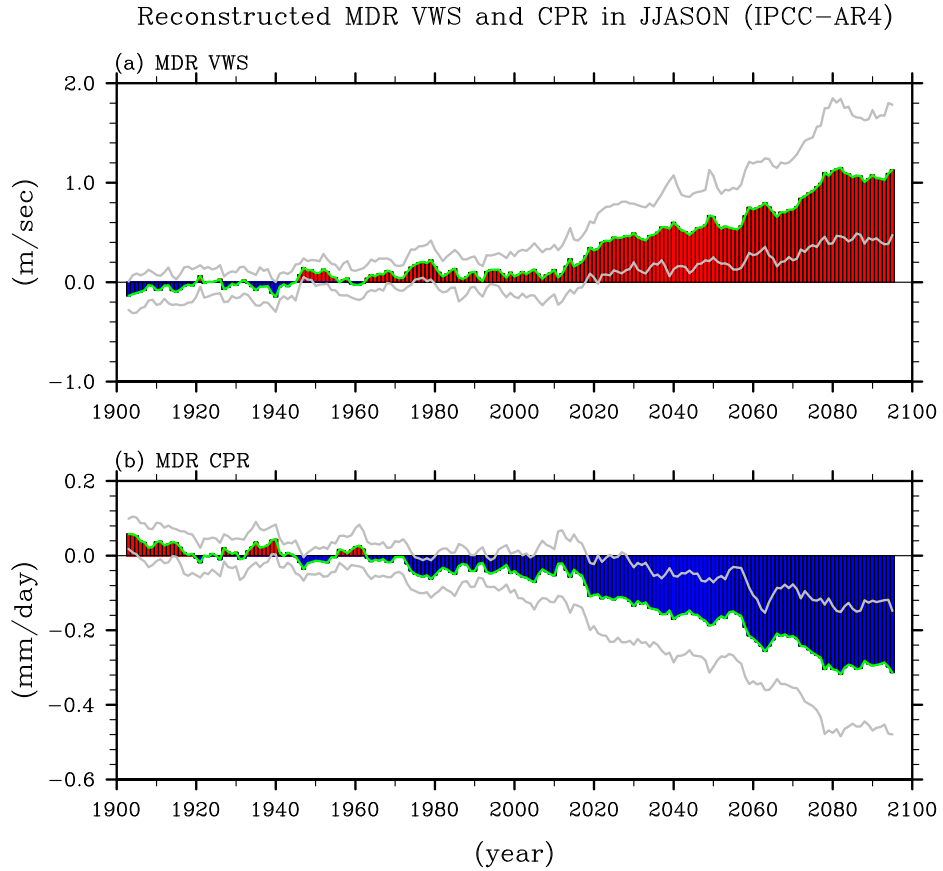


Figure 8. Times series of reconstructed (a) MDR VWS and (b) CPR in JJASON for the period of 1900-2100 based on multiple regressions of the MDR VWS and CPR onto the MDR SST and TIP SST from the ensemble average of 21 IPCC-AR4 climate model simulations under 20C3M and SRESA1B scenarios. Seven-year running mean is applied to all indices before applying the multiple regressions.